AFM and x-ray studies on the growth and quality of Nb(110) on $\alpha$-$Al_2O_3(11\bar{2}0)$



1999 J. Phys.: Condens. Matter 11 2669

(http://iopscience.iop.org/0953-8984/11/13/004)

J. Phys.: Condens. Matter **11** (1999) 2669–2678. Printed in the UK PII: S0953-8984(99)99500-0

# AFM and x-ray studies on the growth and quality of Nb(110) on $\alpha$-$Al_2O_3(11\bar{2}0)$

Bernd Wölfing, Katharina Theis-Bröhl, Christoph Sutter and Hartmut Zabel

Institut für Experimentalphysik/Festkörperphysik, Ruhr-Universität Bochum, D-44780 Bochum, Germany

Received 19 November 1998, in final form 28 January 1999

**Abstract.** We report the effect of annealing of sapphire substrate surfaces and explain the development of step patterns with large terraces. Furthermore, the epitaxial growth of Nb(110) on annealed and unannealed sapphire substrates is studied by AFM and x-ray methods. For the explanation of the well known two component line shape of transverse x-ray scans across Nb(110) Bragg peaks, a structural model is suggested.

## 1. Introduction

Niobium on sapphire often serves as a substrate/buffer system for the epitaxial growth of a large variety of metals. Sapphire substrates are commercially available and are usually of high chemical purity and crystal quality. Nevertheless, there is a remarkable variety of crystal quality among different samples. Since the structural coherence of epitaxial niobium films is limited by the quality of the sapphire template, we have explored possibilities to improve the sapphire properties via annealing. Irrespective of the substrate quality, reports vary as to the proper choice of the Nb film thickness as a buffer for subsequential epitaxial growth. We have therefore investigated the film and structural properties of Nb as they evolve with film thickness.

The sapphire substrates are usually chemo-mechanically polished on one side when purchased. The effect of annealing on the surface morphology was examined via atomic force microscopy (AFM) and x-ray scattering. Subsequently epitaxial Nb films were grown by molecular beam epitaxial (MBE) techniques on pristine and annealed sapphire substrates. We analysed the metal growth behaviour, the structural coherence and the epitaxial relation to the sapphire substrate by AFM and x-ray diffraction as a function of the Nb film thickness and annealing temperature. In the present study we consider only $Al_2O_3(11\bar{2}0)$ substrates and the epitaxial growth of Nb(110) on this substrate. The epitaxial relation between Nb and $Al_2O_3$ is well established and has been described in several places [1–4]. A number of x-ray studies have been devoted to this metal/substrate system with reports on an extraordinary lattice alignment between Nb and sapphire [5], a two component line shape in transverse scans through the (110) Bragg reflection [5–7] and satellite reflections from step ordering [8]. Recent AFM studies revealed mesoscopic surface morphologies that occur on Nb surfaces during epitaxial growth on sapphire substrates with different miscut angles [9].

0953-8984/99/132669+10$19.50  

## 2. Annealing studies of $Al_2O_3(11\bar{2}0)$ substrates

The crystal quality of the substrates was analysed by x-ray diffraction. X-ray transverse scans were taken across the $Al_2O_3(11\bar{2}0)$ Bragg reflection. The angular full width at half maximum ($\Delta\theta^{sapph}_{FWHM}$) reflects the mosaicity of the crystal. Prior to annealing we found $\Delta\theta^{sapph}_{FWHM}$ values in the range $0.01^\circ \leqslant \Delta\theta^{sapph}_{FWHM} \leqslant 0.04^\circ$. The substrates were annealed at temperatures between 1000–1500 °C in air. After annealing at 1500 °C for 12 hours, we found $\Delta\theta^{sapph}_{FWHM} = 0.005^\circ$, corresponding to the resolution limit of our x-ray set up.

AFM topographs of the sapphire surface were taken prior to annealing of the substrate. They showed no distinct features. The surface roughness was less than 1 Å. The $(11\bar{2}0)$ surface was an energetically preferred low-index plane corresponding to one of the equilibrium shapes of the crystal. In the case of a vicinal cut we expected to observe steps and terraces at the surface which brought the surface back to equilibrium [10]. Vicinal surfaces are usually due to polishing procedures and miscut angles between 0.2° and 1° are normal. Since no steps were seen by AFM we concluded that the near surface regions must have been amorphized during polishing [11]. Even after annealing at 1000 °C for six hours no change of the surface morphology was observed with AFM. However, after annealing at 1100 °C we found on the surface the formation of a step pattern (figure 1). The steps had a height of 2.4 Å, corresponding to the distance of two subsequent $O^{2-}$ layers. Since no steps with less height could be detected we considered these as monoatomic steps. The terrace length was about 1 $\mu$m, and its width ranged from 180–260 Å. The direction of the miscut was perpendicular to the average direction of the steps. The step edges were oriented parallel to the $[10\bar{1}0]$ direction and perpendicular to the [0001] direction. With increasing temperature the surface order improved towards a lower number of steps and a rising step height and terrace width. At a temperature of 1500 °C the terrace length exceeded 5 $\mu$m, which is the maximum scan range of our AFM. The terrace width increased to 8000 Å. On these huge terraces we found subterraces due to the still progressing surface ordering, which was only interrupted by cooling the sample down after six hours. The

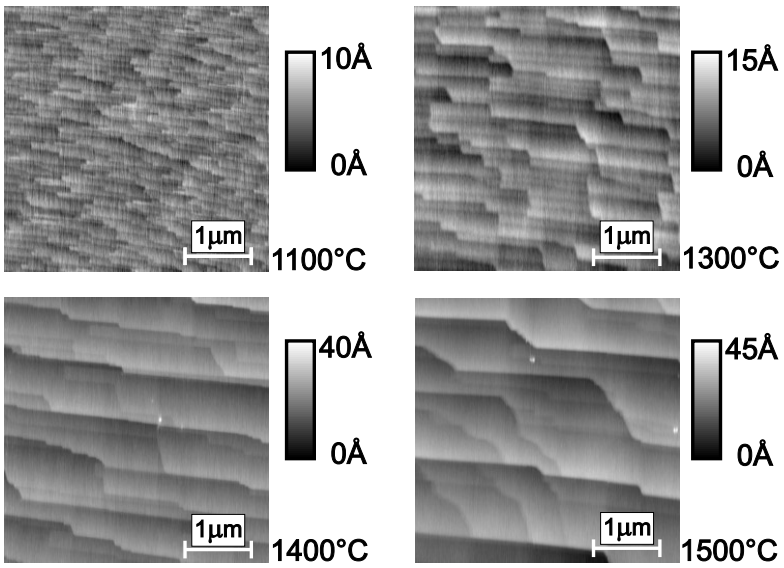


**Figure 1.** AFM pictures showing the development of a step pattern during the annealing in air of sapphire substrates at different temperatures and for six hours.

step height amounted up to 40 Å which corresponds to 16 monolayers. For all annealing temperatures the ratio of the step height to terrace width found from AFM agrees well with the miscut angle observed by x-ray diffraction. Furthermore, the miscut angle did not change during annealing. This indicates that for temperatures up to 1500 °C the surface mobility is too low to allow a mass transport over the entire sample surface, which would be required to reduce the miscut angle. Therefore, the surface processes observed here are of local nature and insufficient to diminish any miscut by annealing.

As shown in figure 1, at first during annealing a step pattern with small terraces separated by monoatomic steps develops from a formerly amorphous surface. With increasing temperature the terraces coalesce and therefore the number of steps decreases. The energetic reason driving this ordering process is the reduction of the edge energy. During annealing the total energy of the crystal, consisting of volume, surface and edge terms, will be reduced. Since the volume and surface contributions do not change during annealing, the total energy can only be lowered by a decreasing step density, i.e. the number of steps per unit area as well as their length. In a first approximation we consider the terrace width to be limited by the diffusivity of the surface particles. Then the dependence of the terrace width $L$ on annealing temperature $T$ and time $t$ is given by the diffusion equation as [12]:

$$D = \frac{L^2}{2t} = D_0 \exp(-E_a/kT)$$

where $E_a$ is an activation energy which describes the bond strength at the surface. The development of terraces at the sapphire surface of width $L$ is well described by this equation. Hence, we conclude that $L$ is limited by surface diffusion. For the sapphire $(11\bar{2}0)$ surface we determined $E_a = (4.3 \pm 0.3)$ eV. Similar studies have only been carried out for sapphire $(10\bar{1}2)$ surface [13], where a binding energy of $E_a = 5$ eV was found. The higher value can be explained by the higher binding energy of the $(10\bar{1}2)$ surface which is energetically the most favourable of all planes.

## 3. Surface morphology of Nb(110) on annealed and unannealed $Al_2O_3(11\bar{2}0)$ substrates

In the second part of this experiment we compared the Nb(110) growth on annealed and unannealed sapphire for different Nb thicknesses by means of AFM measurements. Nb was evaporated with an electron beam gun in our MBE chamber at a substrate temperature of 900 °C [14]. The growth rate was 0.5 Å $s^{-1}$.

After growth of 20 Å Nb on an unannealed $Al_2O_3(11\bar{2}0)$ we found Nb islands with diameters of 200–400 Å and without preferred orientations (see figure 2). These islands seem to nucleate at defects introduced by the miscut or during polishing. In contrast, on annealed

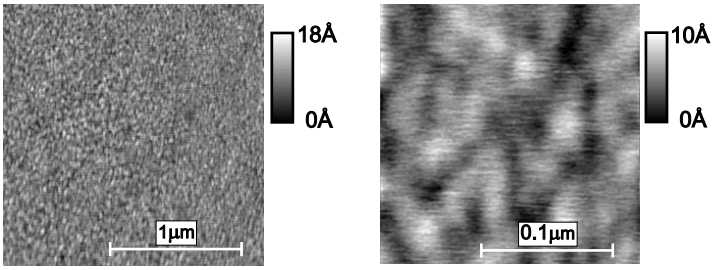


**Figure 2.** AFM pictures taken from a 20 Å thick Nb film grown on an unannealed sapphire substrate. Both pictures represent scans from the same surface by using different scan sizes.

sapphire surfaces the terraces are so smooth and defect free that the Nb atoms arriving on the terraces do not find a nucleation centre. They diffuse over long distances to a step edge and Nb islands grow from there. This is the growth mode originally proposed by Flynn for deriving the optimal substrate temperature during epitaxial growth, which turns out to be $T = 3/8T_M$, where $T_M$ is the melting temperature of the metal [15]. Figure 3 reproduces AFM pictures taken before and after deposition of a thin Nb film on an annealed saphhire substrate. Compared to the sapphire surface shown in figure 1 this sapphire substrate was oriented differently during the polishing of the surface. As a result, the miscuts of both sapphire surfaces point in different directions compared to the crystallographic orientations of the sapphire. Therefore, we find differently shaped step edges after the annealing process. One surface shows steps with sawtooth shaped edges (see figure 3) compared to a finger shaped pattern of the surface steps of the other surface as shown in figure 1. For the deposition experiments we used the sapphire with the sawtooth shaped pattern of the step edges. This pattern changed into a wave shaped pattern during the Nb deposition (figure 3, top pictures). The AFM pattern taken with smaller scan sizes (figure 3, bottom pictures) especially revealed the effect of the coarsening of the sawtooth pattern to a wave shaped pattern. We did not find any isolated Nb islands on the terraces. Therefore, on both sapphire surfaces, annealed or unannealed, the nucleation is heterogeneous.

With larger nominal Nb thicknesses of 200–300 Å the metal surfaces became similar, irrespective of whether grown on annealed or unannealed substrates (figure 4). In the latter case the islands coalesced and a step-like pattern occured with lateral structures of 2000–6000 Å in size. Furthermore, on unannealed substrates the ratio of the step height to the terrace width was smaller than one would expect from the miscut. Since Nb(110) grows on $Al_2O_3(11\bar{2}0)$ without any misorientation, this observation implies that the Nb terraces are inclined with respect to the (110) plane along the miscut direction of the sapphire. On annealed

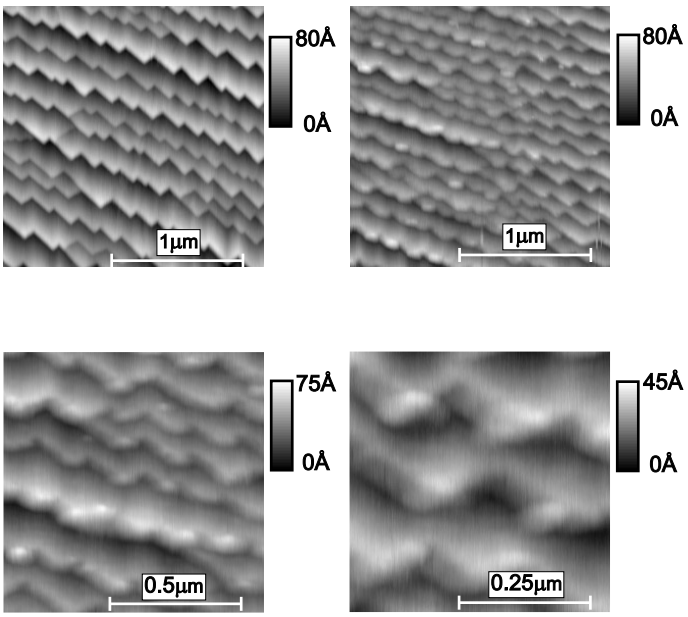


**Figure 3.** AFM pictures taken from an annealed sapphire substrate before (top left) and after deposition (top right) of 20 Å Nb. The pictures below show AFM pictures with smaller scan sizes taken after Nb deposition.

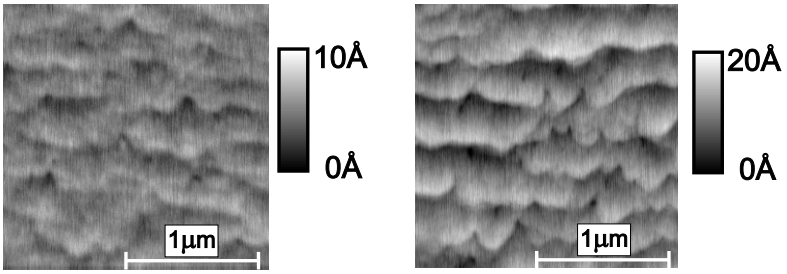


**Figure 4.** AFM pictures taken from Nb films on unannealed (left, 300 Å Nb) and annealed (right, 200 Å Nb) sapphire substrates.

substrates the average terrace width and step height of the sapphire was conserved in the Nb film. However, we observed the development of a meandering of the Nb step edges decorating the originally straight $[10\bar{1}0]$ sapphire terrace edges.

## 4. Structural properties of epitaxial Nb(110) films on sapphire substrates

We have also analysed the crystal structure of the Nb(110) films by x-ray scattering. In figure 5 a partial reciprocal space for Nb(110) on $Al_2O_3(11\bar{2}0)$ and the change of the scattering vector during transverse and radial scans is shown.

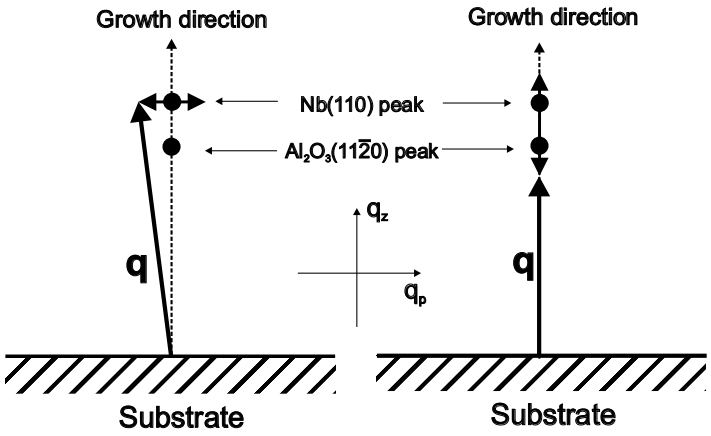


**Figure 5.** Sketch of the reciprocal space with the Nb(110) and $Al_2O_3(11\bar{2}0)$ peaks. The left picture shows the change of the scattering vector during transverse scans and the right picture the change of the scattering vector during radial scans.

We performed transverse (rocking) scans across the centre of the (110), (220) and (330) reflections of the Nb films with a thickness of 330 Å and 770 Å, respectively. Figure 6 shows the intensity of the three scans for the 330 Å thick Nb film. Two distinct features are present in all three scans: a sharp specular component with an angular width of $\Delta\theta^{Nb}_{FWHM} \simeq 0.005^\circ$ and a much broader component with $\Delta\theta^{Nb}_{FWHM} \simeq 0.2^\circ$. This is in line with earlier observations of a two component line shape for Nb(110) in transverse scans of the perpendicular [110] reciprocal lattice rod [5–8]. Furthermore, we determined the width of the Bragg peaks in the radial direction for the sharp and the broad components. In figure 7 are shown two radial scans for the 330 Å thick Nb(110) film. The 'sharp component' was scanned over the maximum

as seen in the transverse scan (see figure 6), while for the scan of the 'broad component' in the radial direction a small off-set angle was used. In both scans the $Al_2O_3(11\bar{2}0)$ peak is seen to the left at about 2.62 $Å^{-1}$ and a broad background peak to the right arising from a thin Pd protection top layer. For the sharp component of the Nb(110) peak we recognize Laue oscillations on both sides, indicative for the high structural order of the film. The sharp and broad components exhibit the same FWHM, corresponding to the whole film thickness of 330 Å and 770 Å, respectively. Consequently, the specular and the broad components do not arise from different parts in the film. There are good reasons why they originate from one and the same part of the film and just reflect different structural orders with two different length scales. This will be discussed further below.

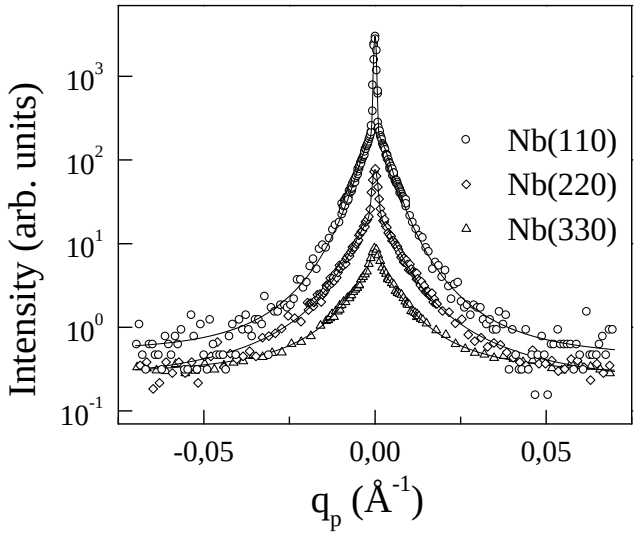


**Figure 6.** Transverse scans across the centre of the Nb(110), (220) and (330) Bragg peaks performed on a 330 Å thick Nb film. The peak intensity decreases with increasing order.

As can be seen in figure 6, with higher order of the {hh0} Bragg reflections the intensity of the sharp component decreases much faster than the intensity of the broad component. The fast intensity drop originates from height–height fluctuations about the average long range orientational order (LROO) [16, 17]. These fluctuations can be described by a lattice roughness parameter $\sigma_{lattice}$, which is the rms height deviation of the scattering planes in the sample. Then the integrated intensity of the sharp component is damped by a Debye–Waller-like roughness factor with increasing scattering vector $Q$ according to $R = \exp(-Q^2\sigma^2)$. We determined the lattice-roughness parameter $\sigma_{lattice}$ for the Nb(110) films taking into account other $Q$-dependent factors such as the absorption factor for thin films, Lorentz factor, polarization factor and a calculated thermal Debye–Waller factor. The values for the two films are:

$$\sigma_{lattice} = 0.21 \pm 0.04 Å$$

for the 330 Å Nb film and

$$\sigma_{lattice} = 0.24 \pm 0.04 Å$$

for the 770 Å Nb film. These values are considerably larger than the thermal contribution to the Debye–Waller factor, for which we calculate a $\sigma_{thermal}$ = 0.13 Å at 300 K.

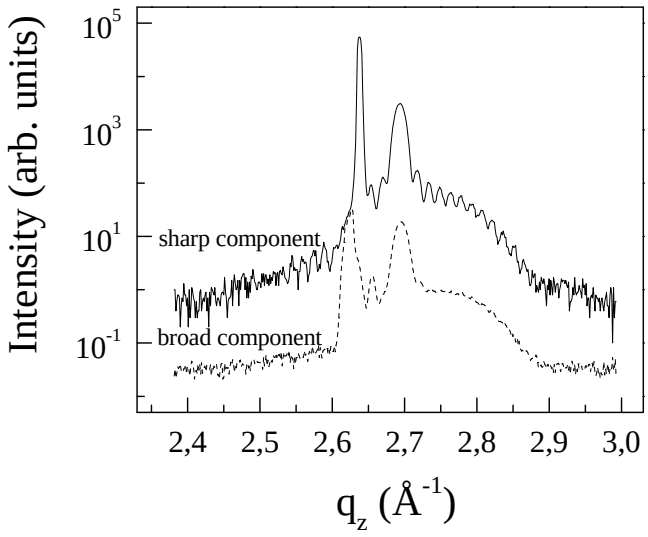


**Figure 7.** Radial scans across the Nb(110) Bragg peak performed on a 330 Å thick Nb film. The scan labeled 'sharp component' was taken across the centre of the transverse peak maximum while the 'broad component' scan was measured with a small transverse offset of $q_p = 0.01$ Å$^{-1}$.

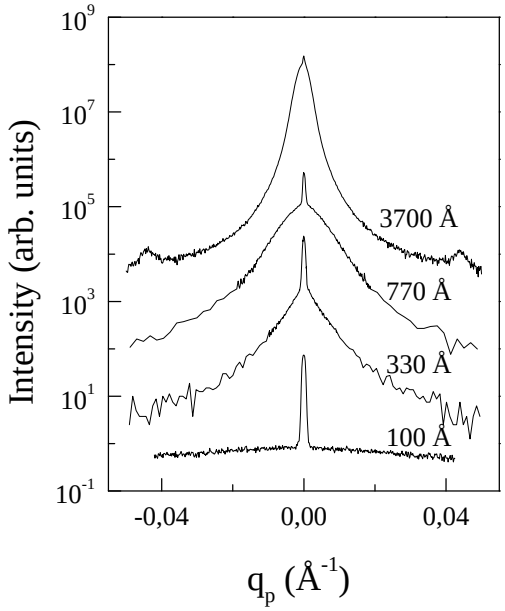


**Figure 8.** Transverse scans through the Nb(110) Bragg reflection and for different niobium thickness.

The two component line shapes of the Nb(110) Bragg peak in the transverse direction are reproduced in figure 8 for Nb film thicknesses from 100–3700 Å. These films were all grown on unannealed substrates. Radial scans across the sharp and broad components confirmed the complete structural coherence for both components over the entire film thickness even for the 3700 Å thick film. The integrated intensity of both components in the transverse direction

increased with film thickness up to 3700 Å. Therefore, LROO is present even for atomic planes grown at distances far from the sapphire interface. However, compared to the broad component, the integrated intensity of the sharp component increases much more slowly. Thus, the ratio of the sharp to the diffuse intensity decreases with increasing layer thickness, which, in turn, implies an increasing $\sigma_{lattice}$ as the metal film grows thicker.

Further information on the crystal structure of the Nb films can be derived from investigating the transverse width of the broad component as it evolves with film thickness. The width decreases with increasing film thickness from approximately $2^\circ$ at a thickness of 100 Å to $0.07^\circ$ at a thickness of 3700 Å. The latter value agrees with the rocking width of high quality bulk crystals [18]. The improving lateral order on the shorter of the two length scales may be either caused by a reduction of the mosaic distribution or an enhanced in-plane coherence length. Because of the simultaneous increase of $\sigma_{lattice}$ in the perpendicular direction, the latter case appears more probable.

We would also like to comment on the satellite peaks around the main reflection of the 3700 Å thick film (see figure 8). These sidebands originate from a periodic distortion of the (110) planes. From the distance of the satellites to the main reflection one can calculate the projection of the periodicity of the distortions to the scattering plane. By rotation of the sample around the azimuth $\phi$ the distance between the main and the satellite reflections changes proportional to $\cos(\phi - \delta)$. For the case $\phi = \delta$ (azimuth $\phi$ is equal to the offset angle $\delta$) the periodic order of the distortions is parallel to the scattering plane. At this azimuth, the periodicity of the distortions can be calculated from the distance of the satellite peaks to the main peak. In the present case, a periodicity of 145 Å was found. We infer, from the position of the satellite peaks, that this periodicity can be explained by the development of a periodic network of lattice distortions due to the lattice mismatch between sapphire and niobium. The average spacing between the additional Nb planes (which have been inserted into the Nb lattice as distortion network) was found to be 20 Å in the [111] and 160 Å in the $[1\bar{1}1]$ direction [19]. For that reason, we assume that the observed distortions originate by this periodic network. The present satellite reflections have to be distinguished from those observed by Gibaud *et al* [8]. In that case, satellites with a much higher spacing of about 2000 Å were observed. They arise if the sapphire is miscut so that its surface forms a regular terrace structure of $(11\bar{2}0)$ planes, and the deposited overlayer has a lattice constant different from the substrate.

## 5. Discussion and growth model

With our x-ray analysis of Nb(110) films on $Al_2O_3(11\bar{2}0)$ we have established so far the following facts:

(1) The rocking curves of $\{hh0\}$ Bragg reflections exhibit a two component line shape, consisting of a well separated sharp and broad components. The $\Delta\theta^{Nb}_{\mathrm{FWHM}}$ value for the sharp component is limited by instrumental resolution.
(2) Independent of the niobium thickness (100–3700 Å) the radial scans through the $\{hh0\}$ Bragg peaks reveal structural coherence lengths extending over the entire film thickness.

These two results can be explained by the growth model illustrated in figure 9. For a large number of Nb crystallites the lattice planes are parallel and in phase, a coherence which is stimulated by the sapphire substrate (dashed line in figure 9). This long range orientational order (LROO) exceeds the length scale of the local order within one crystal domain by orders of magnitude†. The transverse width $\Delta\theta^{Nb}_{FWHM}$ of the specular component, which is only

† It should be noted that by LROO we understand an orientational order with respect to an axis parallel to the film plane and not perpendicular to the film plane as often discussed in the context of hexatic phases.

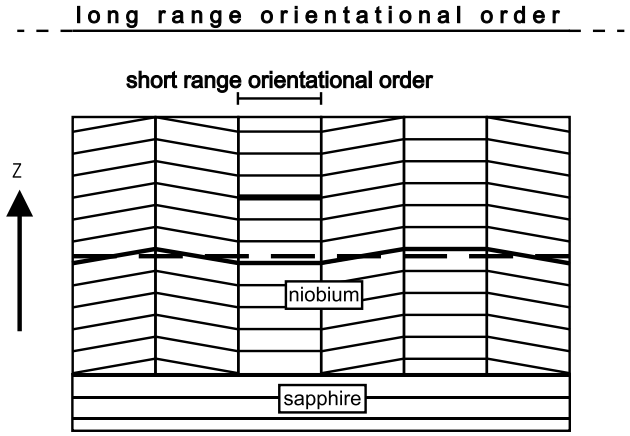


**Figure 9.** The two length scales for orientational order in an epitaxial film grown on a single crystalline substrate is schematically outlined. One order is of long range extending over all crystal domains while the other is of short range and limited to the one particular domain.

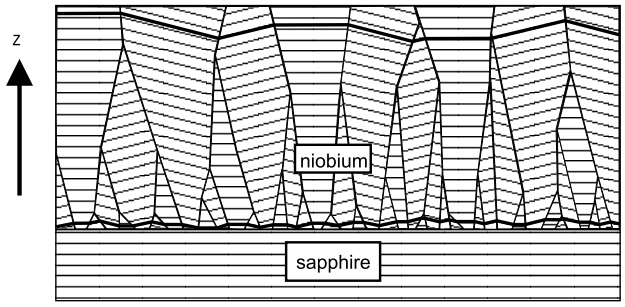


**Figure 10.** Extended model of a niobium epitaxial film with two orientational length scales. With increasing film thickness the long range orientational order is lost due to an increasing mosaicity among the crystal domains. This model can describe the thickness dependence of the two component line shape as observed in the experiments.

limited by instrumental resolution, reflects this LROO and corresponds to a correlation length of at least 25000 Å.

However, there are two more striking observations, which require an extension of our growth model:

(3) With increasing film thickness the integrated intensity of the broad component increases faster than the intensity of the sharp component.
(4) With increasing film thickness the width of the broad component decreases.

In order to account for these additional features, we have to extend our growth model. As shown schematically in figure 10, we assume that the initial growth of Nb on sapphire is of the Vollmer–Weber type, which is justified by the AFM observation of islands. Therefore, the lateral domain size close to the interface is small. With increasing film thickness the islands coalesce, thereby increasing the lateral extension of the domains. This is indicated in figure 10 by the growth of some domains at the expense of others. The lateral expansion of these domains explains the decreasing width of the broad component with increasing film thickness. The remaining large domains still extend over the whole film thickness, giving rise

to the radial width of the Bragg peak in the perpendicular direction. The thick solid lines, following lattice planes close to the interface and further away, illustrate how at the same time the lattice roughness $\sigma_{lattice}$ increases with film thickness and the LROO is lost. This effect finally results in a decrease of the intensity ratio of the sharp to the broad component.

There are two crystal quality parameters of importance to be considered in thin film growth. One concerns the sharp component in transverse scans reflecting long range orientational order on macroscopic length scales. The other is related to the broad component due to the lateral extension of individual domains. While the first diminishes with increasing film thickness, the second grows in intensity and becomes more narrow. Because of their exclusive nature, it is not possible to optimize both parameters at the same time. The optimal film thickness depends on the application of the film. Thin Nb films ($\sim$ 100 Å) with long range orientational order but small domains are suitable as a buffer for epitaxial films which do not rely on pseudomorphic growth, i.e. films with a large lattice misfit to Nb. In this case Nb provides a very flat surface and a template for rotational order. Good examples for this type of growth are Cr(110) [20], Y(0001) [21, 22], and the rare earth metals on Nb(110) [23]. On the other hand, thick films ($\geqslant$ 3000 Å) show a rocking width of the broad component comparable to high quality bulk crystals, but by far a weaker long range orientational order. Such a buffer would be best for high quality pseudomorphic film growth, such as Ta(110), Mo(110) and W(110).

## Acknowledgments

This work was supported by the Deutsche Forschungsgemeinschaft, SFB 166 and by the Ministerium für Wissenschaft und Forschung des Landes Nordrhein–Westfalen, which is gratefully acknowledged.

## References

[1] Durbin S M, Cunningham J E, Mochel J E and Flynn C P 1981 *J. Phys. F: Met. Phys.* **11** L223
[2] Mayer J, Flynn C P and Rühle M 1990 *Ultramicrosc.* **33** 51
[3] Flynn C P 1990 *Metal and Ceramic Interfaces* ed Rühle M *et al* (Oxford: Pergamon) p 168
[4] Gutekunst G, Mayer J and Rühle M 1997 *Phil. Mag.* A **75** 1 329
[5] Reimer P M, Zabel H, Flynn C P and Dura J D 1992 *Phys. Rev.* B **45** 11 426
[6] Zhou G L and Flynn C P 1999 *Phys. Rev.* B **59** at press
[7] Wildes A R, Cowley R A, Ward R C C, Wells M R, Jansen C, Wireen L and Hill J P 1998 *J. Phys.: Condens. Matter* **10** L631–37
[8] Gibaud A, Cowley R A, McMorrow D F, Ward R C C, and Wells M R 1993 *Phys. Rev.* B **48** 14 463
[9] Zhou G L, Bonham S, and Flynn C P 1997 *J. Phys.: Condens. Matter* **9** L671
[10] Herring C 1951 *Phys. Rev.* **82** 87
[11] Beitel G, Markert K, Wiechers J, Hrbek J and Behm R J 1993 *Springer Series in Surface Sciences* vol 33 (Berlin: Springer)
[12] Wang S C and Ehrlich G 1988 *Surf. Sci.* **206** 451
[13] Peng L-M and Czernuszka J T 1991 *Surf. Sci.* **243** 210–8
[14] Bröhl K, Bödeker P, Metoki N, Stierle A and Zabel H 1993 *J. Cryst. Growth* **127** 682
[15] Flynn C P 1988 *J. Phys. F: Met. Phys.* **18** L195
[16] Miceli P F, Weatherwax J, Krentsel T and Palmström C J 1996 *Physica* B **221** 230
[17] Reimer P M 1993 *Thesis* University of Illinois
[18] Metzger H 1975 *Thesis* Technische Universität München
[19] Gutekunst G, Mayer J, Vitek V and Rühle M 1997 *Phil. Mag.* A **75** 1357
[20] Sonntag P, Donner W, Metoki N, and Zabel H 1994 *Phys. Rev.* B **49** 2869
[21] Majkrzak C F, Kwo J, Hong M, Yafet Y, Gibbs D, Chien C L and Bohr J 1991 *Adv. Phys.* **40** 99–189
[22] Remhoff A, Song G, Theis-Bröhl K and Zabel H 1997 *Phys. Rev.* B **56** R2 897
[23] Flynn C P and Salamon M B 1996 *Handbook of the Physics and Chemistry of Rare Earths* vol 22 ed Gschneider K A Jr and Eyring L (Amsterdam: North-Holland)